



Electron injection and interfacial trap passivation in solution-processed organic light-emitting diodes using a polymer zwitterion interlayer



Marta Ruscello^a, Sebastian Stolz^{a, b}, D. Leonardo Gonzalez Arellano^c, Florian Ullrich^{a, d}, Sabina Hillebrandt^{a, e}, Eric Mankel^{a, d}, Annemarie Pucci^{a, e}, Wolfgang Kowalsky^{a, f}, Todd Emrick^c, Alejandro L. Briseno^c, Gerardo Hernandez-Sosa^{a, b, *}

^a InnovationLab, Speyerer Strasse 4, 69115 Heidelberg, Germany

^b Light Technology Institute, Karlsruhe Institute of Technology, Engesserstrasse 13, 76131 Karlsruhe, Germany

^c Department of Polymer Science and Engineering, University of Massachusetts, 120 Governors Drive, Amherst, MA 01003, United States

^d Technische Universität Darmstadt, Materials Science Department, Surface Science Division, Jovanka-Bontschits-Straße 2, 64287 Darmstadt, Germany

^e Kirchhoff-Institut für Physik, Universität Heidelberg, Im Neuenheimer Feld 227, 69120 Heidelberg, Germany

^f Institut für Hochfrequenztechnik, Technische Universität Braunschweig, Schleinitzstrasse 22, 38106 Braunschweig, Germany

ARTICLE INFO

Article history:

Received 3 May 2017

Received in revised form

18 July 2017

Accepted 16 August 2017

Available online 18 August 2017

Keywords:

Poly(sulfobetaine methacrylate)

Zinc oxide

Electron injection layers

OLEDs

ABSTRACT

Here we describe the use of a polymer zwitterion as a solution-processable material that serves as the key component of the electron injection layer (EIL) in solution processed organic light-emitting diodes (OLEDs). Poly(sulfobetaine methacrylate) (PSBMA) was employed in both regular and inverted device configurations as a work-function modifier for Al and ZnO cathodes, respectively. For both architectures, PSBMA significantly improved the OLED performance when compared to reference devices without EIL in terms of turn-on voltage and luminance. In inverted devices, PSBMA showed a passivation effect on ZnO surface trap states, producing better performing and more stable devices.

© 2017 The Authors. Published by Elsevier B.V. This is an open access article under the CC BY license (<http://creativecommons.org/licenses/by/4.0/>).

1. Introduction

One of the most attractive features of solution-processable organic electronic materials is the possibility of using printing or coating technologies for fabricating of optoelectronic components. These high-throughput technologies will allow the low-cost integration of devices such as organic light-emitting diodes (OLEDs), organic field-effect transistors (OFETs), and organic photodetectors (OPDs) into flexible displays, wearables, and sensors, etc. through a reduced energy consumption process [1–3]. A common challenge in device engineering is to select materials with suitable energy matching (i.e., between a metal electrode and semiconductor) in order to avoid energy losses, while simultaneously allowing for sequential deposition of solution-processed layers.

Recent reports show promise in reducing charge injection/extraction energy barriers at interfaces to afford devices with lower operating voltages [4–7]. In solution-processed OLEDs, efforts have been focused on commonly used electron-injection layers based on low work function (WF) alkaline earth metals or alkali metal halides. Such materials are applied by evaporation, have poor chemical stability in ambient conditions, and therefore are incompatible with printing/coating techniques [6]. A promising alternative approach is to combine solution-processable organic/polymer materials with metal cathodes, such as aluminum or silver, as electron injection layer (EILs). For this purpose, conjugated polyelectrolytes and amine-rich polymer have been found to exhibit control over electrode WF and consequently improve device performance [7–12]. Conjugated polyelectrolytes are also adaptable to multilayered device architectures, due to their orthogonal solubility in polar solvents relative to solvent used for active layers. Zwitterionic polymers offer the advantage of being dipole-rich but electrically neutral, containing no mobile ionic species which could

* Corresponding author. Light Technology Institute, Karlsruhe Institute of Technology, Engesserstrasse 13, 76131 Karlsruhe, Germany.

E-mail address: gerardo.sosa@kit.edu (G. Hernandez-Sosa).

negatively affect the stability of devices [13]. The use of conjugated polymer zwitterions as interlayer in OLEDs and solar cells has recently been reported, showing WF reduction of up to 1 eV and improved photovoltaic performance [12–16].

Here we report poly(sulfobetaine methacrylate) (PSBMA) an air stable, electronically neutral, solution-processable zwitterionic polymer as a cathode modification layer in OLEDs. PSBMA was utilized previously in high-efficiency inverted organic solar cells in which the dipole-bearing functionality lowers the work function of the electrode [17]. In this work, we observe that PSBMA not only reduces the WF of Al and ZnO, enabling lower operational voltages, but also serves as a surface trap passivation for ZnO, stabilizing the device under operating conditions. The devices and thin films were characterized by luminance-current-voltage (LIV) curves, Kelvin Probe (KP), X-Ray photoelectron spectroscopy (XPS), Fourier transform infrared reflection absorption spectroscopy (FT-IRRAS), and atomic force microscopy (AFM) to investigate the PSBMA layer morphological and electronic properties.

2. Materials and methods

2.1. Sample preparation

PSBMA was synthesized as described elsewhere [17]. PSBMA solutions were prepared by dissolving the polymer in tri-fluoroethanol in a concentration range from 0.1 to 1 mg ml⁻¹. PSBMA solutions were then spincoated with $\omega = 4000$ rpm, $a = 1000$ rpm s⁻¹, and $t = 45$ s. ZnO nanoparticles (Nanograde N10, 2.5 % wt in 2-propanol) were filtered with a 0.2 μ m PTFE filter, spincoated on the ITO substrates (spin-coating parameters $\omega = 4000$ rpm, $a = 1000$ rpm s⁻¹, and $t = 45$ s so that a layer of about 30 nm was obtained) and annealed on a hot plate at 150 °C for 5 min in a glovebox directly connected to the evaporation chamber, so that the samples did not get in contact with air. Aluminum (100 nm) was evaporated on glass substrates in a vacuum system with a base pressure of 2×10^{-7} mbar.

2.2. OLED preparation

Glass/ITO substrates were subsequently cleaned in Acetone and 2-propanol under sonication for 15 min, respectively, and treated by O₂ plasma for 5 min. Afterward, for regular architecture devices PEDOT: PSS solution (Heraeus PVP Al 4083) was filtered with a 0.45 μ m PVDF filter, spin-coated in ambient conditions and annealed on a hot plate at 135 °C for 15 min. Spin-coating parameters were $\omega = 3800$ rpm, $a = 800$ rpm s⁻¹ and $t = 30$ s so that a layer of about 30 nm was obtained. For inverted devices, ZnO and PSBMA were deposited as described before. SuperYellow (light emitting polymer), acquired from Merck KGaA, was dissolved in Toluene with a concentration of 5 mg ml⁻¹ and spin-coated in a glovebox. Spincoating parameters were $\omega = 2000$ rpm, $a = 1000$ rpm/s and $t = 45$ s and delivered a layer thickness of approximately 70 nm. Afterward, the samples were annealed on a hot plate located inside a glovebox at 115 °C for 30 min. In case of the reference OLEDs, 10 nm of Ca followed by 100 nm of Al were evaporated as cathode layer in a vacuum system with a base pressure of 1×10^{-7} mbar. Finally, 100 nm of aluminum were evaporated as cathode. For inverted devices, 10 nm of MoO₃ followed by 100 nm of Al were evaporated on top of the emitting polymer as anode layer in a vacuum system with a base pressure of 1×10^{-7} mbar.

2.3. Characterization

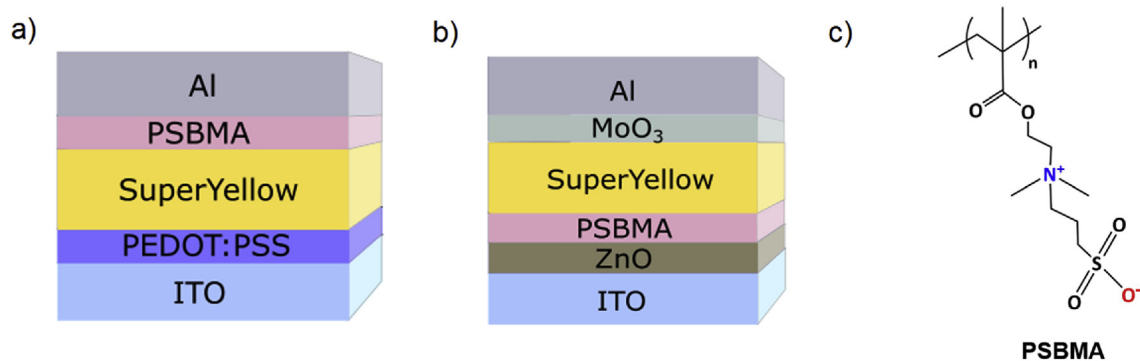
The Kelvin probe characterization was performed using a KP020

single point Kelvin probe system by KP Technology. The system was equipped with a gold tip with a diameter of 2 mm, and its energetic resolution is ~ 20 meV. The photoelectron spectroscopy characterization was performed using a PHI VersaProbe II scanning XPS microprobe. The spectrometer is equipped with a monochromatized Al-K_z X-ray source, an Omicron HIS 13-helium discharge lamp, and a concentric hemispherical analyzer. Detail spectra of the core level lines were recorded with a pass energy of 11.75 eV, for the secondary electron edges 0.58 eV were chosen. The spectra and secondary electron edges are referenced in binding energy with respect to the Fermi edge and the core level lines of in situ cleaned Ag, metal foil. AFM images were recorded with a DME DS 95 Dualscope AFM in ambient conditions in tapping mode using highly doped silicon cantilevers from NanoWorld (Arrow NCR). These cantilevers have resonance frequencies of about 285 kHz and tip radii of less than 10 nm. IR reflection absorption spectra were obtained in the nitrogen purged sample compartment of a Bruker Vertex80v Fourier-transform (FT) IR spectrometer using p-polarized light and an angle of incidence of 75° with respect to the surface normal. A liquid nitrogen cooled mercury cadmium telluride (MCT) detector was used and all spectra are the average over 200 scans that were taken with a resolution of 4 cm⁻¹. Each measurement was divided by a background spectrum of a clean ITO or ZnO/ITO substrate, thus giving the relative reflectance of the investigated layer.

3. Results and discussion

To evaluate the suitability of PSBMA as an electron injection layer in light-emitting devices, solution-processed OLEDs were prepared in both regular and inverted architectures, utilizing a PPV-derivative, commonly known as SuperYellow (SY), as the emissive layer. As EIL, spin-coated films of PSBMA with different thicknesses were used and their performance was compared to the bare aluminum electrode for the regular architecture, and to a single ZnO layer for the inverted architecture (Scheme 1). Due to the small amount of deposited material we were not able to determine the PSBMA layer thickness with sufficient accuracy neither by profilometry, AFM or ellipsometry measurements on top of the emissive layer or the ZnO nanoparticles. Therefore, in this work we will refer to the PSBMA concentration in solution as an indirect measure of layer thickness.

Fig. 1 presents the LIV-characteristics of the prepared devices as well as the typical OLED figures of merit as a function of PSBMA concentration (*i.e.* layer thickness). For devices with a regular architecture (Fig. 1a and c), it can be observed that the presence of PSBMA increases the device performance for concentrations below 0.6 mg ml⁻¹ compared to devices containing a pristine Al cathode. An optimal PSBMA concentration of 0.25 mg ml⁻¹ results in a turn-on voltage (V_{on} , here defined at a luminance of 1 cd m⁻²) of 2.23 V and a current efficiency of 4.2 cd A⁻¹, with a maximum luminance of $\sim 10^4$ cd m⁻² at 10 V. The observed ten-fold improvement in luminance values compared to the pristine Al cathode is accompanied by a reduction of current density, suggesting more balanced hole- and electron currents. On the one hand, the reduced WF of PSBMA/Al should increase electron injection since it is observed to decrease operating voltages, however, the total current decreases. On the other hand, the hole injection is the same for both samples, leading to the conclusion that the reduction in total current comes from holes being blocked by the PSBMA layer thus increasing exciton formation probability and resulting in the observed luminance increase. The characterization of the unipolar devices for both charge carriers confirms that the presence of PSBMA in the device causes a lower hole current and three orders of magnitude higher electron current,



Scheme 1. Device architectures for regular OLEDs (a) and inverted OLEDs (b); chemical structure of PSBMA (c).

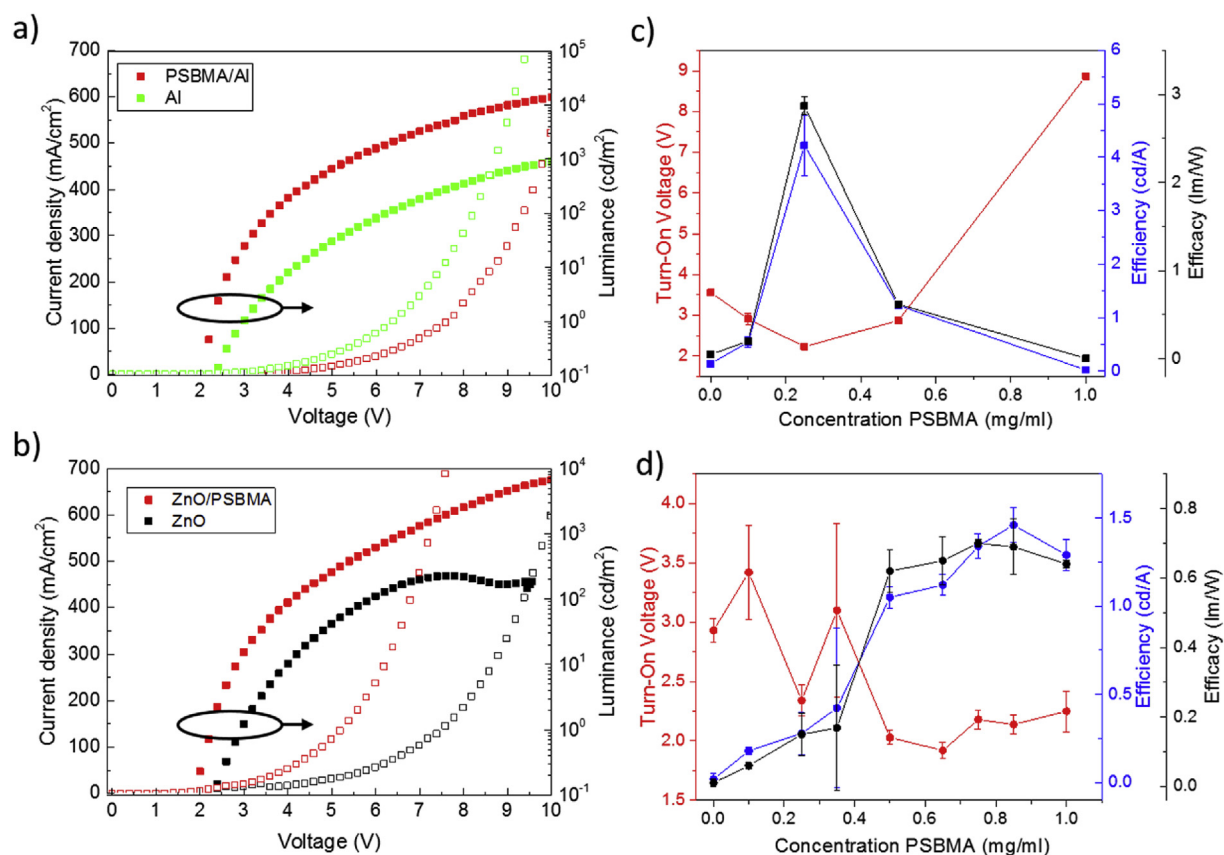


Fig. 1. LIV-characteristics and main device parameters as a function of PSBMA concentration. In a) and b) devices with regular and inverted architectures with optimal PSBMA concentrations are compared to devices with no EIL. Each data point in c) and d) is the average of at least four devices.

respectively (see Fig. S2). Compared to a device with Ca/Al cathode, the PSBMA/Al cathode injects a lower electron current, which being not balanced with the higher hole current injected by the PEDOT:PSS results in an overall lower device current, and therefore a lower efficiency (see Fig. S1). In the case of devices with an inverted architecture (Fig. 1b and d), the optimal concentration of PSBMA was 0.85 mg ml⁻¹. At this concentration, the OLEDs exhibit a $V_{on} = 2.14$ V and a maximum current efficiency of 1.46 cd A⁻¹. These values represent ~0.9 V reduction in operational voltages, with a luminance almost two orders of magnitude higher than devices containing pristine ZnO as the EIL. This improvement is directly related to the higher current density enabled by more

efficient electron injection from the PSBMA/ZnO layer. It has reported that solvent washing with pure solvents, especially alcohols, can positively affect the performance of organic electronic devices [18,19]. In order to rule out the possibility that the PSBMA carrying solvent (i.e. trifluoroethanol (TFE)) induces this effect, we fabricated solvent-washed devices in both regular and inverted architectures. Devices where ZnO or SY were treated with pure TFE exhibited comparable performances to the reference devices without any solvent treatment. The complete characterization and comparison of the device performance as a function of PSBMA thickness and solvent treatment is presented in Fig. S1 and Tables S1 and S2 of the SI.

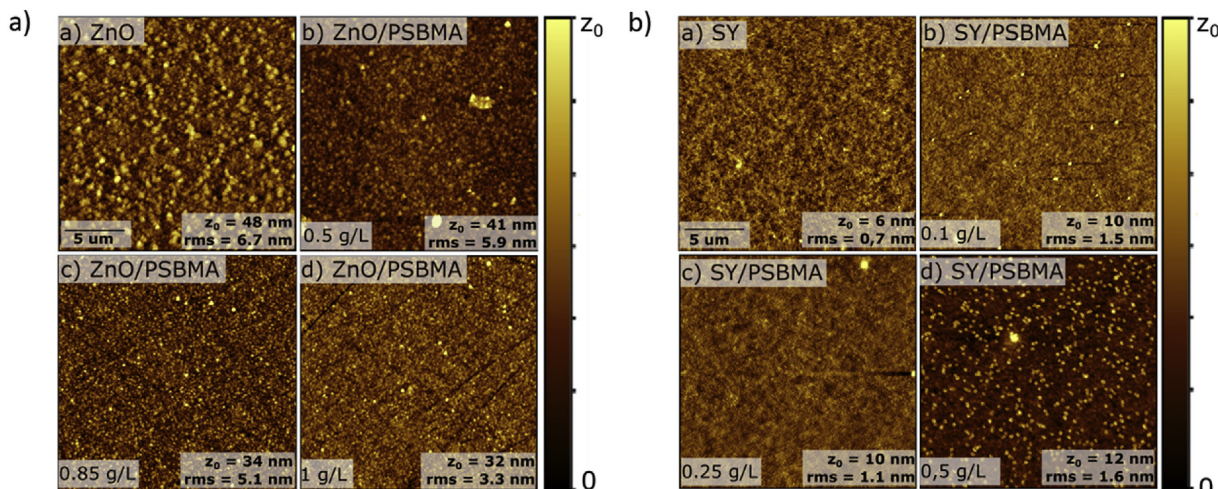


Fig. 2. AFM images of PSBMA in various concentrations on top of a) ZnO and b) Super Yellow, the emitting polymer. (For interpretation of the references to colour in this figure legend, the reader is referred to the web version of this article.)

Fig. 2a shows AFM images of ZnO and PSBMA-coated ZnO. The initial rms roughness of the ZnO film (6.7 nm) is reduced by the PSBMA layer (3.3 nm), leading to a more favorable morphology for deposition of the emissive layer. The optimum PSBMA concentration of 0.85 mg ml⁻¹ presented an rms value of 5.1 nm. In contrast to ZnO, SY forms a smooth film with low surface roughness, as shown in Fig. 4b. The optimal concentration of PSBMA used for device fabrication (0.25 mg ml⁻¹) does not alter the roughness of the resultant film significantly (rms from 0.7 to 1.1 nm). However, at a concentration of 0.5 mg ml⁻¹, drop-like clusters of PSBMA distributed evenly over the measured area had a detrimental effect on charge injection, as suggested by the relative device performances.

KP measurements were used to determine the work function of PSBMA-coated Al and ZnO films. Fig. 3 shows that the WF of ZnO and Al settle around ~4 eV and ~3 eV, respectively, when the PSBMA concentration (*i.e.*, thickness) is increased. The WF shifts in case of the optimal concentrations in devices are -278.6 meV (0.85 mg ml⁻¹) for ZnO and -123.1 meV (0.25 mg ml⁻¹) for Al. The decreasing WF trend with PSBMA thickness is consistent with prior

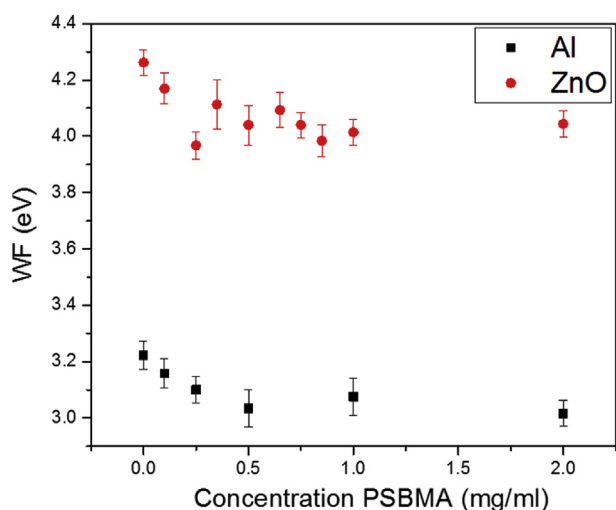


Fig. 3. Work-function of aluminum and ZnO samples covered with PSBMA layers of different thicknesses measured by Kelvin Probe.

studies and comparable in magnitude to other polymeric systems [17,20,21]. In the present case, the optimum PSBMA concentration for the best device performance resulted from a trade-off between WF shift, suitable film morphology and minimized EIL resistivity due to the insulating nature of PSBMA. Furthermore, we performed ultraviolet and x-ray photoelectron spectroscopy (UPS and XPS) on Al/PSBMA and ZnO/PSBMA samples (Fig. S3). For PSBMA on Al and ZnO we measured a WF of 2.94 eV and 3.40 eV, respectively, in good correlation with the KP results. XPS was used to determine the PSBMA layer thickness for the concentrations used in the best performing OLEDs through the damping of the Al and Zn core level peaks as detailed in the SI. Assuming a homogeneous coverage, the nominal PSBMA layer thickness was determined as 2.1 nm and 0.8 nm for Al (0.25 mg ml⁻¹) and ZnO (0.85 mg ml⁻¹), respectively. The PSBMA layer on top of ZnO was expected to be thicker. However, due to the ZnO surface roughness (see Fig. 2) it is very likely that the PSBMA layer is not homogeneous, in which case the calculated nominal thickness would be much smaller than the average thickness. No reliable thickness value could be estimated on top of SY.

Fig. 4a shows the behavior of V_{on} after consecutive measurements using a voltage ramp of 0–10 V on devices with ZnO, PSBMA and PSBMA/ZnO as EIL. The other figures of merit of the device (*i.e.* efficiency and efficacy) follow the same trend as V_{on} (see Fig. S4). The V_{on} of the PSBMA-only devices steadily increased until device failure after 10 runs, indicating a rapid degradation of the device. For ZnO-only devices, V_{on} decreases gradually until it reaches a stable value after ~11 runs, showing that the multiple voltage ramps have an activation effect on the cathode. This V_{on} reduction can be related to the gradual occupation of electron traps in ZnO [22] which usually originates from surface defects of the ZnO nanoparticles [23,24]. Interestingly, devices with a ZnO/PSBMA EIL show a ~60% drop in V_{on} after the first voltage ramp and keep stable operation conditions until the twentieth measurement. This behavior suggests the ability of the PSBMA layer to passivate the surface trap states of the ZnO nanoparticle layer. These surface defects are sensitive to the presence of certain functional groups [25], as a quaternary amine, carboxyl, or the sulfonate group present in PSBMA, and could thus be passivated by a capping layer of PSBMA. This effect is also evident in Fig. 4b where a pre-bias of 2 V was imposed for 10 min prior to the LIV measurement. The current efficiency of the device with pristine ZnO increased by 20 times advertising that the pre-bias helps filling ZnO trap states and

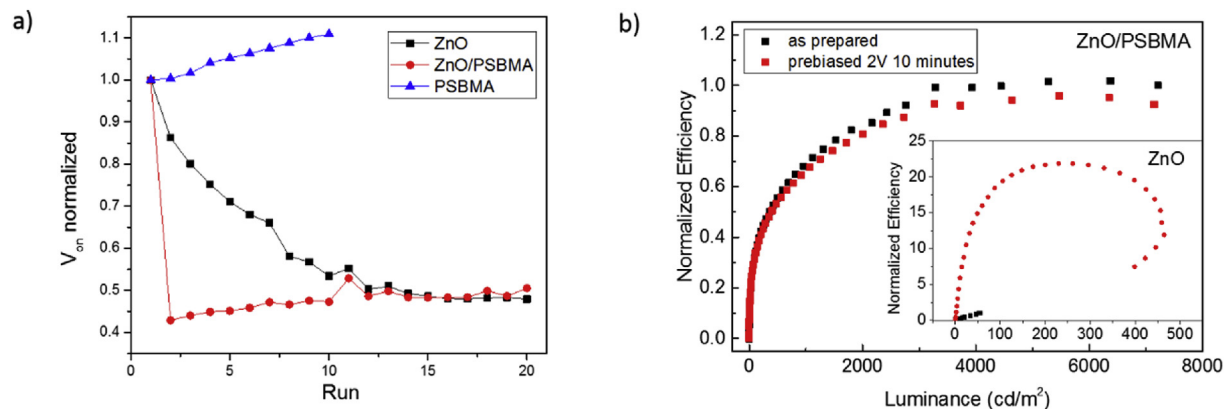


Fig. 4. Electrical stress measurements for devices using ZnO, PSBMA and PSBMA/ZnO as EIL. a) Normalized turn-on voltage for consecutive LIV measurements on the same device. The voltage ramp was set from 0 to 10 V; b) Normalized current efficiency before and after a pre-bias of 2 V for 10 min (the ZnO-only device is presented in the inset).

facilitates electron injection into the active layer. On the contrary, devices where ZnO was capped with PSBMA do not show a significant difference after the pre-bias demonstrating that the surface states responsible for the electron traps were passivated by PSBMA. The same electrical stress measurements were conducted on devices with a regular architecture, showing that such trap-passivation occurred at ZnO/PSBMA interface and PSBMA did not passivate the aluminum interface (see Fig. S5). FT-IRRAS measurements were conducted on ITO, ITO/ZnO, ITO/ZnO/PSBMA and ITO/PSBMA samples (see Fig. S6). IR spectroscopy indicated that PSBMA replaces the adsorbates present on a pristine ZnO surface. As the adsorbates on the nanoparticulate ZnO mostly contain oxygen, the replacement may lead to a reduction of trap states at the interface.

4. Conclusions

In summary, we demonstrated the use of the zwitterionic polymer PSBMA as EIL in solution-processed OLEDs in regular, as well as inverted, architecture. Characterization of the PSBMA thin films by AFM, KP and XPS revealed that the polymer forms a thin, smooth film, and reduced the WF of Al and ZnO down to a value of ~ 3 eV and ~ 4 eV, respectively. For both architectures, the PSBMA interlayer significantly improved OLED V_{on} by up to ~ 1 V when compared to reference devices. In particular, for the inverted architecture, PSBMA remarkably improved the surface morphology of the nanoparticulate ZnO film and passivated its surface trap states, leading to a more stable device operation. The dual function of PSBMA as WF modifier and trap passivation could be applicable to a wider range of multilayer optoelectronic devices with hybrid interfaces.

Acknowledgements

This work was financially supported by the EC through the Horizon 2020 Marie Skłodowska-Curie ITN project INFORM (Grant Agreement 675867). A.L.B acknowledges the Office of Naval Research (ONR N00014-16-1-2612). The authors are grateful to S. Beck for fruitful discussion.

Appendix A. Supplementary data

Supplementary data related to this article can be found at <http://dx.doi.org/10.1016/j.orgel.2017.08.014>.

References

- [1] H. Klauk, *Organic Electronics. More Materials and Applications II*, Wiley, 2012.
- [2] S. Raupp, D. Daume, S. Tekoglu, L. Merklein, U. Lemmer, G. Hernandez-Sosa, H.M. Sauer, E. Dörsam, P. Scharfer, W. Schabel, *Adv. Mater. Technol.* (2016) 1600230.
- [3] G. Hernandez-Sosa, N. Bornemann, I. Ringle, M. Agari, E. Dörsam, N. Mechau, U. Lemmer, *Adv. Funct. Mater.* 23 (2013) 3164.
- [4] Z. Yin, J. Wei, Q. Zheng, *Adv. Sci.* 3 (2016) 1.
- [5] N. Koch, *ChemPhysChem* 8 (2007) 1438.
- [6] T. Chiba, Y.-J. Pu, J. Kido, *J. Mater. Chem. C* 3 (2015) 11567.
- [7] S. Stolz, M. Petzoldt, S. Dück, M. Sendner, U.H.F. Bunz, U. Lemmer, M. Hamburger, G. Hernandez-Sosa, *ACS Appl. Mater. Interfaces* 8 (2016) 12959.
- [8] C. Sun, Z. Wu, H.L. Yip, H. Zhang, X.F. Jiang, Q. Xue, Z. Hu, Z. Hu, Y. Shen, M. Wang, F. Huang, Y. Cao, *Adv. Energy Mater.* 6 (2016) 1.
- [9] O. Kim, B. Kang, J. Lee, S. Lee, S. Cha, J. Lee, S. Kim, S. Kim, S. Kang, *IEEE Electron Device Lett.* 37 (2016) 1022.
- [10] J. Wang, K. Lin, K. Zhang, X.F. Jiang, K. Mahmood, L. Ying, F. Huang, Y. Cao, *Adv. Energy Mater.* 6 (2016).
- [11] F. Huang, H. Wu, Y. Cao, *Chem. Soc. Rev.* 39 (2010) 2500.
- [12] Z.A. Page, V.V. Duzhko, T. Emrick, *Macromolecules* 46 (2013) 344.
- [13] Y. Liu, V.V. Duzhko, Z.A. Page, T. Emrick, T.P. Russell, *Acc. Chem. Res.* 49 (2016) 2478.
- [14] J. Fang, B.H. Wallikewitz, F. Gao, G. Tu, C. Müller, G. Pace, R.H. Friend, W.T.S. Huck, *J. Am. Chem. Soc.* 133 (2011) 683.
- [15] W. Zhang, C. Song, X. Liu, J. Fang, *ACS Appl. Mater. Interfaces* 8 (2016) 18593.
- [16] C. Duan, L. Wang, K. Zhang, X. Guan, F. Huang, *Adv. Mater.* 23 (2011) 1665.
- [17] H. Lee, E. Puodziukynaite, Y. Zhang, J.C. Stephenson, L.J. Richter, D. a Fischer, D.M. Delongchamp, T. Emrick, A.L. Briseno, *J. Am. Chem. Soc.* 137 (2015) 540.
- [18] F. Jiang, W.C.H. Choy, X. Li, D. Zhang, J. Cheng, *Adv. Mater.* 27 (2015) 2930.
- [19] H. Zhou, Y. Zhang, J. Seifert, S.D. Collins, C. Luo, G.C. Bazan, T.Q. Nguyen, A.J. Heeger, *Adv. Mater.* 25 (2013) 1646.
- [20] Y. Lee, J. Wang, S.R. Cheng, J.W.P. Hsu, *ACS Appl. Mater. Interfaces* 5 (2013) 9128.
- [21] H.C. Chen, S.W. Lin, J.M. Jjiang, Y.W. Su, K.H. Wei, *ACS Appl. Mater. Interfaces* 7 (2015) 6273.
- [22] A.J. Morfa, B.I. Macdonald, J. Subbiah, J.J. Jasieniak, *Sol. Energy Mater. Sol. Cells* 124 (2014) 211.
- [23] A.J. Morfa, N. Kirkwood, M. Karg, T.B. Singh, P. Mulvaney, *J. Phys. Chem. C* 115 (2011) 8312.
- [24] G.A. Beane, A.J. Morfa, A.M. Funston, P. Mulvaney, *J. Phys. Chem. C* 116 (2012) 3305.
- [25] N.S. Han, H.S. Shim, J.H. Seo, S.Y. Kim, S.M. Park, J.K. Song, *J. Appl. Phys.* 107 (2010).